Facile approach for surfactant-free synthesis of Au@ginsenoside Rh$_2$ nanoparticles and researches on anticancer activity

Hua Yao[1†], Xupeng Mu[1†], Zhenhong Wei[1], Xiuying Li[1], Liya Wu[1], Yongri Jin[2], Xuwen Li[2], Jing Li[1*] and Jinlan Jiang[1*]

†Hua Yao and Xupeng Mu play the equal contribution to the article and should be co-first authors

*Correspondence:
lijing1029@jlu.edu.cn;
jiangjinlan@jlu.edu.cn

[1] Scientific Research Center, China-Japan Union Hospital of Jilin University, Changchun 130033, People's Republic of China
[2] College of Chemistry, Jilin University, Changchun 130021, People's Republic of China

Abstract

Background: Inorganic nanocomposites especially Au nanostructures have exhibited outstanding physicochemical properties in biomedical fields. For further clinical applications on theranostics, especially drug delivery, numerous explorations of green and facile synthesis methods combining with pharmacoactive natural components have been investigated to construct safe and multifunctional bioactive Au nanoparticles (NPs). Ginsenoside Rh$_2$ is protopanaxadiol type compound isolated from plants of genus *Panax*, with excellent anticancer effect and antioxidant activity. In this research, we prepared the novel Au nanoparticles using ginsenoside Rh$_2$ as both reducing and stabilizing agents.

Results: The synthesized Au@ginsenoside Rh$_2$ NPs were proved to exhibit desirable inhibitory effect on different cancer cell lines, which benefited from the inherent anticancer effect of the ginsenoside Rh$_2$. Investigations in vitro indicated that Au@ginsenoside Rh$_2$ NPs inhibited cell proliferation, cell migration and invasion, induced cell cycle arrest, enhanced the reactive oxygen species (ROS) generation, and regulated the protein expressions of caspase-3, 8, 9 to trigger cell apoptosis as well.

Conclusions: Because of the absence of toxic chemical surfactants, the eco-friendly synthesis method of Au NPs modified by natural phytochemicals avoided tedious separation and modification processes. On the other hand, Au@ginsenoside Rh$_2$ NPs also improved water solubility and bioavailability of the hydrophobic drug ginsenoside Rh$_2$. It broadened minds for preparation and application of traditional Chinese medicines (TCMs) modified metal nanoparticles and deserved further study.

Keywords: Ginsenoside Rh$_2$, Au nanoparticles, Drug-modified nanocomposite, Facile synthesis, Anticancer activity

Introduction

Severe toxic and side effects, poor prognosis or easy palindromia, disadvantages of certain conventional cancer therapies cause discomfort and further injury to patients (Brown et al. 2021; Zheng et al. 2018). With rapid development of nanotechnology and the advent of the century of life science, numerous researchers have dedicated to explore

safer and more effective ways combining with nanomaterials to improve innovative cancer cures (El-Sahli et al. 2021; Liu et al. 2020a; Wang et al. 2021). Owing to the unique structures and enhanced performances, metal nanocomposites, especially Au nanoparticles (NPs) have attracted increasing attention in biomedical fields (Alphandery 2020; Ding et al. 2020a; Khursheed et al. 2022; Kuchur et al. 2020). The reported novel multifunctional Au-based nanosystems could not only reduce side effect and improve bioavailability as well as the pharmacodynamic functions of loaded drugs or biomolecules (Ding et al. 2020b; Giraldez-Perez et al. 2021; Rao et al. 2018), but also have considerable potential value on multimodal bioimaging and developing approaches like photothermal and photodynamic therapy (Li et al. 2020b; Liu et al. 2020b; Yang et al. 2021). Therefore, it is a great challenge to create more valuable Au nanodevices that are constructed on the basis of rational designs for precise integration of the applicable specific functional properties of NPs.

In the ever-expanding field of design and fabrication research on Au nanomaterials, most of the conventional methods still confront problems such as safety risks of chemical poisonous reagents participation, complicated multistep preparation and imperative modifications for functions and biocompatibility (da Silva et al. 2020; Fratoddi 2017; Tarantola et al. 2011). On one aspect, some frequently-used surfactants like cetyltrimethylammonium bromide (CTAB) and reductants such as hydrazine hydrate and sodium borohydride ($NaBH_4$) should be carefully removed or coated with biocompatible ligands or shells necessarily for their explicit toxicity (Cheung et al. 2012; Ginzburg et al. 2018; Kumar et al. 2019). Therefore, for avoiding toxic risks and exploiting abundant biomedical applications, more creative explorations on simple and feasible methods are in urgent needs.

Green approaches for Au NPs synthetic methods based on specific natural products have been proposed as a wonderful and alternative ways to improve synthesis method and enhance functionalities of final materials, which should benefit from mild reaction process, avoidance of toxic chemicals use and the pharmacological properties inherent in natural products. In view of the diversity of natural products, different kinds of fruit juice, honey and various plant or fungus extracts have been widely considered to be applied in Au NPs synthesis (Al Saqr et al. 2021; Khan et al. 2019; Qiao and Qi 2021; Ronavari et al. 2021). In current study, the effective phytochemicals in herbal medicines such as curcumin, resveratrol and epigallocatechin gallate (EGCG) etc. have been attracted more attention and developing gradually (Matur et al. 2020; Wang et al. 2017; Wu et al. 2018). Their unique structures and physicochemical characteristics are capable of reducing Au ions into Au NPs and endowing the new materials with special functions.

In this investigation, we employed the natural tetracyclic triterpenoid compound ginsenoside Rh$_2$ from *Panax ginseng* C.A. Meyer as reducing and stabilizing agent. As a kind of ancient and famous Traditional Chinese medicines (TCMs), *Panax ginseng* C.A. Meyer has been used as medicinal plant in China for centuries (Ratan et al. 2021; Ru et al. 2015). Ginsenoside Rh$_2$, which mainly isolated from the rhizome of steamed *Panax ginseng*, belongs to the group of protopanaxadiol type ginsenosides and has been used for natural cancer chemoprevention and treatment agent clinically (Li et al. 2020c). It has also been demonstrated to have various desirable pharmacological activities such as neuro and cardioprotection (Hou et al. 2018; Wang et al. 2012a), antiallergic (Park

et al. 2003), antiobesity (Hwang et al. 2007), antidiabetes (Wang et al. 2012b), antioxidation (Lu et al. 2018) and anti-inflammatory effects (Hsieh et al. 2018), etc. Researchers especially focused on the marvelous anticancer effect and have proved that ginsenoside Rh_2 can inhibit cell proliferation, induce cell apoptosis and cell cycle arrest, and suppress migration and invasion (Li et al. 2020a; Nag 2012). It will also affect different signaling pathways on inhibiting various cancer cells like breast carcinoma, colorectal cancer and leukemia cells (Wang et al. 2019b; Zhang et al. 2021; Zhu et al. 2021). Treatment with ginsenoside Rh_2 at certain concentration will induce prooxidative effect and ROS-mediated cytotoxicity on some cancer cells (Wang et al. 2019b; Zhang et al. 2021; Zhu et al. 2021). However, low bioavailability of ginsenoside Rh_2, which results from its poor aqueous solubility, has restricted its deep applications in clinical. Inspired by the antioxidant activity of ginsenoside Rh_2 on normal cells like macrophages and keratinocytes (Choi et al. 2013), we speculate that ginsenoside Rh_2 may perform reducibility on Au ions to improve the bioavailability and even the anticancer effect. In addition, due to the complexity of contents and constituents in the natural extract of plants with different producing areas and growth ages, application of monomeric compound with certain structure may have better repeatability and stability, compared with the synthesis of metal nanoparticles using medicinal plants extract (Boomi et al. 2019; Hurh et al. 2017; Wang et al. 2019a). The combination of the pharmacological efficacious drug ginsenoside Rh_2 with Au nanoparticles can overcome the disadvantages of water solubility and enhance its cancer inhibition activities and therapeutic efficacy.

In consequence, this investigation aims to improve the bioavailability and anti-tumor activity of water-insoluble ginsenosides Rh_2 by constructing nanocomposites materials. Bioactive compound ginsenoside Rh_2 from *Panax ginseng* C.A. Meyer acts as both reducing and stabilizing agent in the reaction with $HAuCl_4$ for preparing the Au@ginsenoside Rh_2 NPs. The obtained Au@ginsenoside Rh_2 NPs inherit the excellent anticancer effect of ginsenoside Rh_2 and improve the poor water solubility of ginsenoside Rh_2. The in vitro experiments indicated the promising anticancer effect of Au@ginsenoside Rh_2 NPs by cytotoxicity, cell apoptosis, cell cycle, migration assays and expressions of apoptosis-related protein caspase-3, 8, 9. We propose to exert the advantages of pharmacological active natural compound ginsenoside Rh_2 on the synthesis of Au nanoparticles and expect to obtain an improved therapeutic nanosystem with clinical feasibility in future. And we also hope to promote the further applications of TCM-derived constituents in nanomedicine and cancer therapy.

Results and discussion

Synthesis and characterization of Au@ginsenoside Rh_2 NPs

Au@ginsenoside Rh_2 NPs were synthesized by the seed-mediated method. The process includes synthesis of citrate-stabilized Au nanoparticles as seeds and reduction of $HAuCl_4$ with ginsenoside Rh_2 in the presence of Au seeds. Au seeds with diameters at 30–40 nm were initially obtained by reduction the $HAuCl_4$ using citrate in the 100 °C condition. Figure 1A showed the schematic illustration of Au@ginsenoside Rh_2 NPs. In a typical synthesis of Au@ginsenoside Rh_2 NPs, Au seeds were added into the 10 mL double distilled water at room temperature under stirring. Then, $HAuCl_4$ and the ginsenoside Rh_2 with the feeding molar ratio at 10:3 were added into the solution system for

Yao *et al. Cancer Nanotechnology*   (2022) 13:35

Page 4 of 18
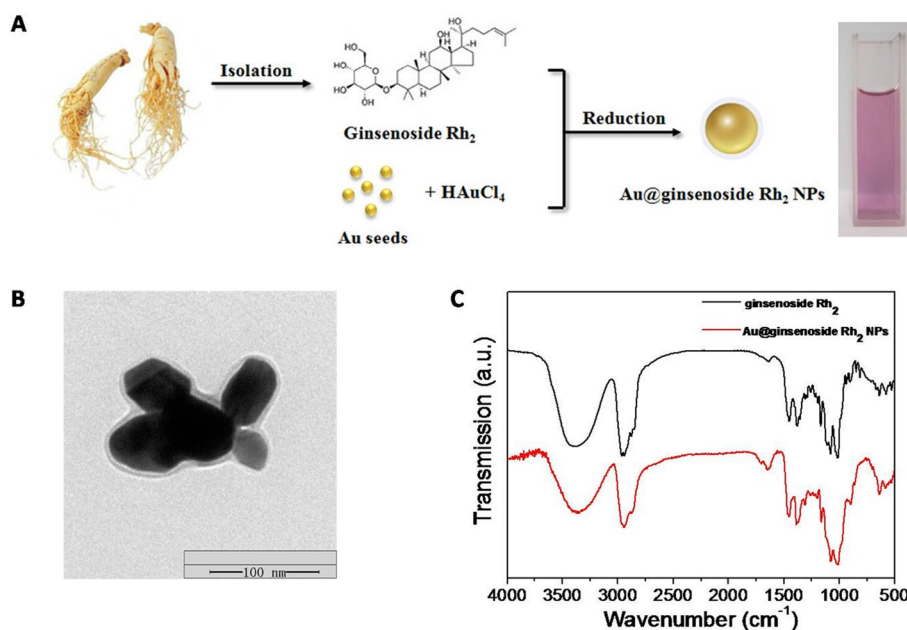
Fig. 1 Schematic illustration of the synthesis of Au@ginsenoside Rh_2 NPs (**A**); TEM image (**B**), the FT-IR spectra of Au@ginsenoside Rh_2 NPs (**C**). The amounts of $HAuCl_4$, ginsenoside Rh_2 and the aqueous solution of Au seeds were taken according to the optimized condition

2 h reaction until the solution turned to violet. The obtained Au@ginsenoside Rh_2 NPs with the average diameter of 70 ± 10 nm were exhibited in Fig. 1B. The zeta potential of the as-prepared NPs was detected at -17.8 mV, indicating the good structure stability. The color of original Au seeds and final color of solution after reaction were shown in Additional file 1: Fig. S1. For Fourier-transform infrared (FT-IR) spectra were measured to confirm the Au@ginsenoside Rh_2 NPs coating with ginsenoside Rh_2. As shown in Fig. 1C, the peaks at 3400–3300 cm^{-1} can be assigned to the hydroxyl stretching vibration of ginsenoside Rh_2. Peaks at 2941 and 2877 cm^{-1} result from the C–H stretching vibration. The weak peak around 1640 cm^{-1} is stretching vibration of C=C structure. Peaks at about 1453–1380 cm^{-1} are corresponding to the bending vibration of H–C–H and H–O–C. And the peaks at 1168, 1079, 1014 cm^{-1} are assigned to the C–O and C–C stretching vibration. Peak at 1108 cm^{-1} is the bending vibration of O–H. The FT-IR analysis of the Au@ginsenoside Rh_2 NPs also exhibited the characteristic peaks of ginsenoside Rh_2, only with slight shift of several wave numbers, which revealed the sufficient combination of ginsenoside Rh_2 on the surface of the Au nanoparticles (Fu et al. 2013). Additional file 1: Figure S2 showed the water solubility enhancement of Au@ginsenoside Rh_2 NPs. Obvious state of suspension could be observed when ginsenoside Rh_2 dissolved in water, while the Au@ginsenoside Rh_2 NPs solution exhibited excellent monodispersity.

The effect of ginsenoside Rh_2 on formation of the Au@ginsenoside NPs was investigated by altering the molar ratio of $HAuCl_4$ and ginsenoside Rh_2 from 10:1 to 10:3. In Additional file 1: Fig. S3, the size of the obtained NPs increased from 60 to 70 nm, while the corresponding UV–vis absorption was shift from 546 to 552 nm. Then we measured the cytotoxicity of the prepared NPs on cancer cells, feeding ratio of $HAuCl_4$ and

ginsenoside Rh_2 at 10:3 showed the best anticancer activity on cancer cells which displayed in Additional file 1: Fig. S4. After comprehensive consideration, we finally take this optimized method as model to prepare Au@ginsenoside Rh_2 NPs and take research on the anticancer effect.

In order to investigate the content of residual ginsenoside Rh_2 after reaction, we tested the synthesis system solution by HPLC under the condition of rare ginsenosides analysis to investigate the possible existence of ginsenoside Rh_2 or any other rare ginsenosides like ginsenoside Rk_2, Rh_3 and PPD derived from ginsenoside Rh_2. HPLC analysis result was shown in Additional file 1: Fig. S5. It indicated that ginsenoside Rh_2 had fully reacted with $HAuCl_4$ and participated in the formation of Au nanoparticles. And there is no free ginsenoside Rh_2 detected in the supernatant after the reaction.

Cell uptake and cytotoxicity of Au@ginsenoside Rh_2 NPs in vitro

After labeled with FITC and incubated with cancer cells A375 for 24 h, the as-prepared Au nanoparticles were proved to be endocytosed by cells via fluorescence microscope imaging. Results were shown in Additional file 1: Fig. S6. The dosage of Au@ginsenoside Rh_2 NPs was 40 μg/mL and green light of FITC could be observed in A375 cells. The fluorescent imaging indicated that the Au@ginsenoside Rh_2 NPs could be accumulated around the cytoblast.

The cytotoxicity of the Au@ginsenoside Rh_2 NPs was investigated by CCK-8 assay after incubating with different cancer or normal cells for 24 h. Results were shown in Fig. 2A. Au@ginsenoside Rh_2 NPs had significant anticancer effect on A549, A375, HepG-2 and U251 cancer cells. However, the Au@ginsenoside Rh_2 NPs represented low cytotoxicity on normal cells 293T and HUVEC. This might provide an extensive application prospect of Au@ginsenoside Rh_2 NPs in cancer therapy. We also compared the anticancer activity of Au@ginsenoside Rh_2 NPs and corresponding loading amount of free ginsenoside Rh_2 on A375 cancer cells. The results showed ginsenoside Rh_2 had a negligible anticancer effect in accordance with the drug loading of the corresponding Au@ginsenoside Rh_2 nanoparticles in Additional file 1: Fig. S7, which demonstrated that Au@ginsenoside Rh_2 NPs had improved the anticancer effect on cancer cells.
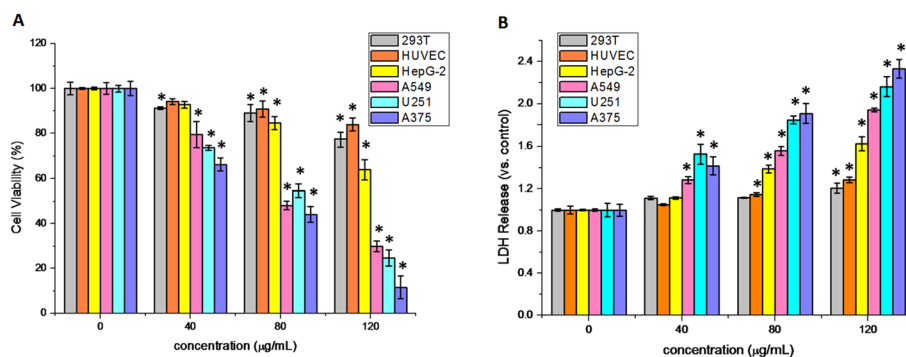
Fig. 2 A Cell viability of different cancer cell lines A375, A549, U251, HepG-2 and normal cells 293T and HUVEC treated with Au@ginsenoside Rh_2. **B** The LDH release of normal cells and cancer cells induced by different concentration of Au@ginsenoside Rh_2 NPs. The values represent mean $\pm$ SD ($n = 3$, $*p < 0.05$, vs control). The results of LDH release are also shown as a relative O.D. value to control group (0 μg/mL)

LDH release was another way to reflect the toxicity of Au@ginsenoside Rh$_2$ NPs on different cells. LDH is a stable cytoplasmic enzyme which will release to the culture media when cell damage occurs. In order to further support the Au@ginsenoside Rh$_2$ NPs induced apoptosis and cell damage, determination of LDH release by normal and cancer cells cultured with different concentrations of Au@ginsenoside Rh$_2$ NPs was necessary. As shown in Fig. 2B, Au@ginsenoside Rh$_2$ NPs induced LDH release from 6 cell lines to different extents. The highest level could be observed in group of A375 cells. The effects of Au@ginsenoside Rh$_2$ NPs in inducing LDH release from normal cells 293T and HUVEC were much lower than other cancer cell lines. The LDH release assay and CCK-8 results provided a comprehensive statement that Au@ginsenoside Rh$_2$ NPs had inhibition effects on certain cancer cells and low toxicity on normal cells.

Effect of Au@ginsenoside Rh$_2$ NPs on cell apoptosis and ROS generation in cancer cells

For further investigating the cytotoxicity of Au@ginsenoside Rh$_2$ NPs on cancer cells, we applied flow cytometry (FCM) to evaluate cell apoptosis associated with the as-prepared nanomaterials. Melanoma A375 cells was chosen as the cancer cells models resulting from their most sensitive effect to Au@ginsenoside Rh$_2$ NPs. Au@ginsenoside Rh$_2$ NPs at the concentrations of 0, 40, 80 and 120 μg/mL incubated with A375 cells. Results were shown in Fig. 3A to demonstrate the contribution of Au@ginsenoside Rh$_2$ NPs during the apoptosis process. The B1-B4 areas represent death, late apoptosis, viability, and early apoptosis of cells, respectively. Compared with the control group, Au@ginsenoside Rh$_2$ NPs could significantly induce cell apoptosis especially the late apoptosis status. 2.4%, 12.9%, 55.6%, 65.3% of the A375 cells were found at the late apoptosis stages with the increasing concentration of as-prepared nanoparticles. This indicated that cell apoptosis of A375 cells was triggered by the presence of Au@ginsenoside Rh$_2$ NPs and in a dose-dependent manner with concentration.

Increasing of intracellular reactive oxygen species (ROS) was considered to relate with cell apoptosis. Therefore, Au@ginsenoside Rh$_2$ NPs-mediated ROS production was detected by the FCM assay using DCFH-DA fluorescent probes. Results showing in Fig. 3B confirmed that Au@ginsenoside Rh$_2$ NPs induced ROS excessive generation in A375 cells. ROS level of A375 cells were raised from 56.1 to 85.5% with the increasing concentration of Au@ginsenoside Rh$_2$ NPs incubated for 24 h. It indicated that the Au@ginsenoside Rh$_2$ NPs-induced imbalance of ROS leads to oxidative stress-mediated apoptosis.

High-content imaging analysis for anticancer potential of cancer cells treated with Au@ginsenoside Rh$_2$ NPs

In order to further investigate cell apoptosis and necrosis after incubating A375 cells with Au@ginsenoside Rh$_2$ NPs, Hoechst/PI double-staining method was applied in this experiment. PI could not enter the cells with normal construction of the cell membrane, while Hoechst 33342 could penetrate the cell membrane into cells. So when bright blue and weak red fluorescence could be observed, apoptosis was thought to have occurred. Existence of necrosis would be reflected when cells showed weak blue and bright red fluorescence. High-content cell imaging analysis could successfully complete to get pictures by the Operetta CLS™ system from PerkinElmer Inc.
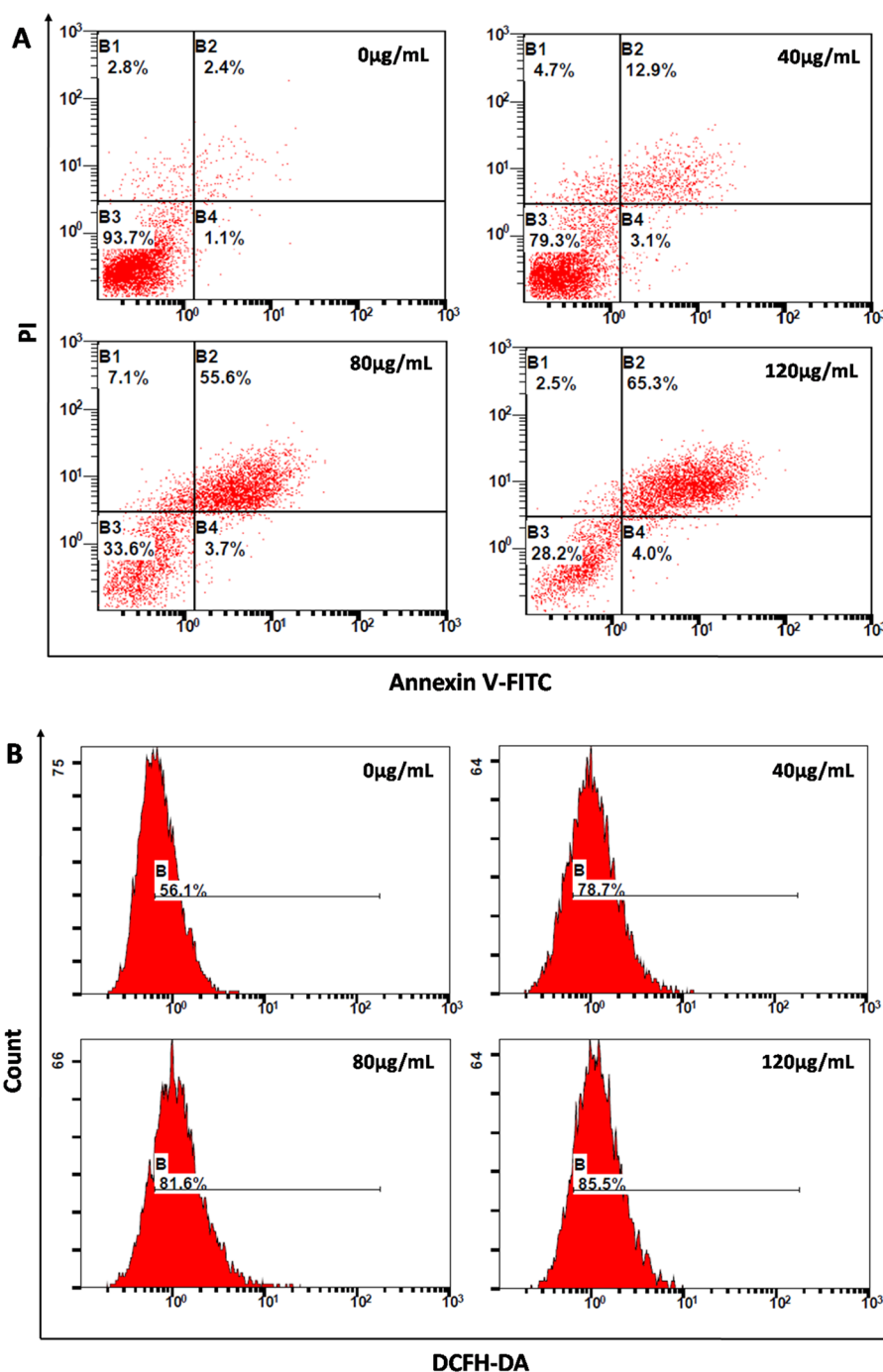
Fig. 3 Cell apoptosis (**A**) and ROS generation (**B**) of A375 cells treated with different concentration of Au@ ginsenoside Rh$_2$ NPs

Results shown in Fig. 4A exhibited merged dual-color fluorescence with the increasing concentration of Au@ginsenoside Rh$_2$ NPs, which meant cell apoptosis and damage enhancement could be observed obviously when incubated with Au@ginsenoside Rh$_2$ NPs for 24 h. We also tried to directly reflect the correlation between ROS and
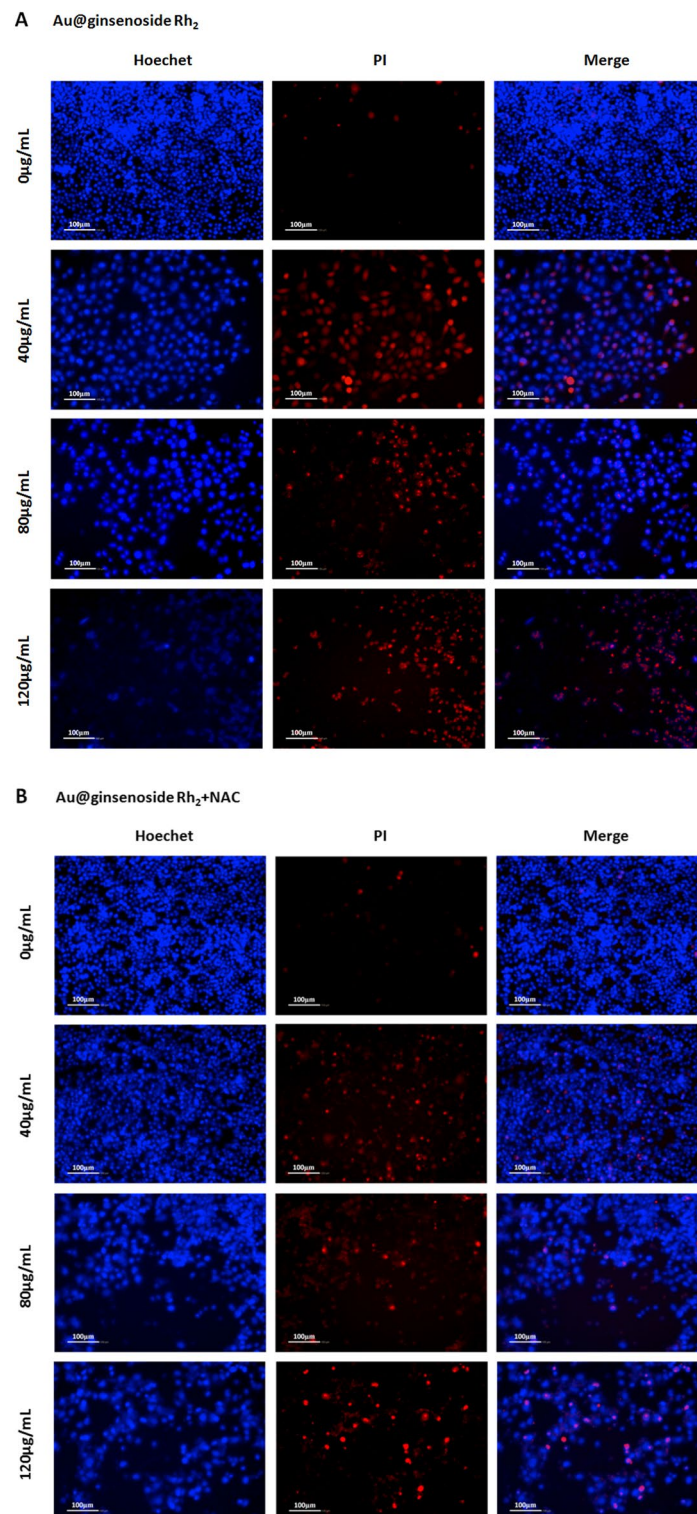
Fig. 4 High-content imaging analysis of A375 cells apoptosis and necrosis treated only with Au@ginsenoside Rh$_2$ NPs (**A**) and that under the co-existence of antioxidant *N*-acetyl-ʟ-cysteine (NAC) and Au@ginsenoside Rh$_2$ NPs condition (**B**)

apoptosis via fluorescent imaging. So we introduced 10 mmol/L ROS scavenger NAC and different concentrations of Au@ginsenoside Rh_2 NPs into the system and co-incubated with A375 cells for 24 h. The images in Fig. 4B revealed that cell apoptosis was inhibited when NAC was added in the Au@ginsenoside Rh_2 NPs-treated system, apparently. It indicated that NAC decreased the generation of ROS and thus influenced apoptosis of A375 cells.

The above results demonstrated that Au@ginsenoside Rh_2 NPs were capable of inhibiting cancer cell proliferation and inducing apoptosis through the ROS-mediated pathway. But some extent of apoptosis was still found in Au@ginsenoside Rh_2 NPs + NAC groups, which suggested that Au@ginsenoside Rh_2 NPs might also cause apoptosis though other pathways.

Au@ginsenoside Rh_2 NPs caused migration and invasion inhibiting on cancer cell in vitro

In order to investigate whether the Au@ginsenoside Rh_2 NPs would inhibit the metastatic potential of cancer cells, wound scratch and transwell assays were taken as description. Images were taken at 0 h and 24 h after incubating A375 cells with Au@ginsenoside Rh_2 NPs. As shown in Fig. 5A, the wound width of control group (0 µg/mL) was significantly decreased after 24 h culture, while wound width of A375 cells treated with different concentrations of Au@ginsenoside Rh_2 NPs had little change. Figure 5B showed the quantitative description of the width variation (*$p < 0.01$, vs control). Transwell assay results in Fig. 5C, D showed that cell number passing through the membrane was significantly reduced after being treated with Au@ginsenoside Rh_2 NPs compared with the control group. Both above data indicated that Au@ginsenoside Rh_2 NPs exhibited certain inhibiting effect of migration and invasion on A375 cells in vitro.
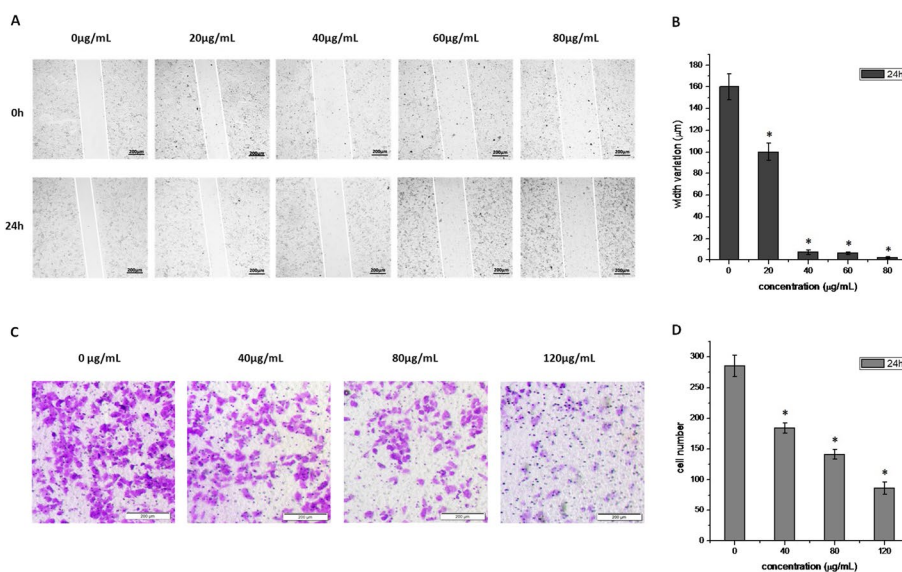
Fig. 5 Migration ability of A375 cancer cells after treated with different concentrations of Au@ginsenoside Rh_2 NPs by wound scratch assay (**A**); Quantitative results of wound width variation of A375 cells in 24 h (**B**); Invasion of A375 cells after co-culture with Au@ginsenoside Rh_2 NPs for 24 h measured by transwell assay (**C**); quantitative results of A375 cell numbers in transwell assay (**D**). *$p < 0.01$, compared with control group

Cell cycle arrest analysis of Au@ginsenoside Rh₂ NPs treated with cancer cells

Cell cycle analysis could further investigate the relations about cell viability, proliferation and apoptosis of cancer cells influenced by Au@ginsenoside Rh₂ NPs. Cell cycle progression of A375 cells cultured with different concentrations of Au@ginsenoside Rh₂ NPs was examined using FCM. Analysis results were shown in Fig. 6. G1, S and G2/M phase of regular growing cancer cells without nanoparticles stimulating (control group, 0 μg/mL) were 77.57%, 9.51% and 12.92% proportion, respectively. With the increasing concentration (40, 80, 120 μg/mL) of Au@ginsenoside Rh₂ NPs treated with A375 cancer cells for 24 h, G1 phase proportion decreased to 57.86%, 33.04%, 32.70% and the S phase were raised to 22.94%, 57.99% and 60.51% proportion, respectively. Proportion of G2/M phase was also moderately decreased after incubating with Au@ginsenoside Rh₂ NPs. Results indicated that the as-prepared Au NPs would cause cell cycle arrest at S phase, which meant that synthesis of DNA and cell cycle progression of A375 had been inhibited significantly combining with other detections.

Western blot analysis for anticancer effect of Au@ginsenoside Rh₂ NPs

In order to elucidate whether the anticancer effect of Au@ginsenoside Rh₂ NPs was associated with cell apoptosis at protein level, expression of caspase-3, 8, 9 was detected
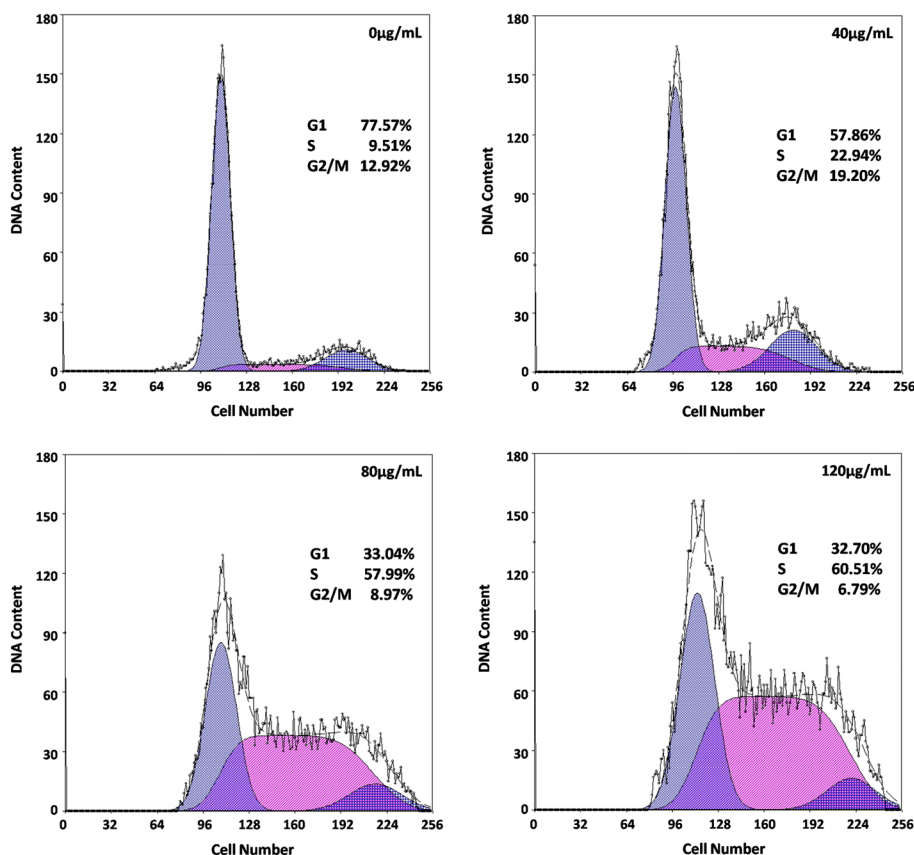
Fig. 6 Cell cycle distribution analysis of different concentrations of Au@ginsenoside Rh₂ NPs affected on A375 cancer cells

by western blot analysis. Western blot results in Fig. 7A, B showed that the expressions of caspase-3, 9 were down regulated and cleaved caspase-3, 9 could be detected with increasing concentration of Au@ginsenoside Rh_2 NPs. The decreased expression of caspase-8 in A375 cells after incubating with different concentrations of Au@ginsenoside Rh_2 NPs could also be observed. The gray scale values of samples were displayed in Fig. 7C, D as quantitative results of western blot (*$p < 0.05$). It would be more accurate and direct to illustrate the existence of cell apoptosis by comparing the gray value ratios of caspase-3, 8, 9 related objective protein vs internal reference (β-actin), which were calculated by Image J program. Based on the western blot results, we suggest that Au@ginsenoside Rh_2 NPs are able to induce cancer cell apoptosis by caspase-mediated signaling pathway.

Conclusion

In summary, we have developed a green synthesis approach for Au@ginsenoside Rh_2 NPs as the ginsenoside Rh_2 acting as reducing and stabilizing agents without the poison surfactants helping. We regulated the conditions and finally optimized the synthesis process by controlling the feeding of $HAuCl_4$ and ginsenoside Rh_2 at the molar ratio of 10:3 under room temperature for 2 h reaction. As ginsenoside Rh_2 have promising anticancer activity, the as-prepared Au@ginsenoside Rh_2 NPs not only improved the water solubility properties of the ginsenoside Rh_2 via the synthesized way with Au nanoparticles in one hand, but also endowed the Au@ginsenoside Rh_2 NPs with desirable biocompatibility and inherent cancer inhibition capability from ginsenoside Rh_2. In vitro investigations confirmed that the Au@ginsenoside Rh_2 NPs would promote intracellular ROS generation and induce apoptosis through ROS and caspase-mediated signaling pathway. They also played an important role in cell cycle arrest, migration and invasion inhibition of cancer cells. These findings are critical to the understanding of the synthetic and
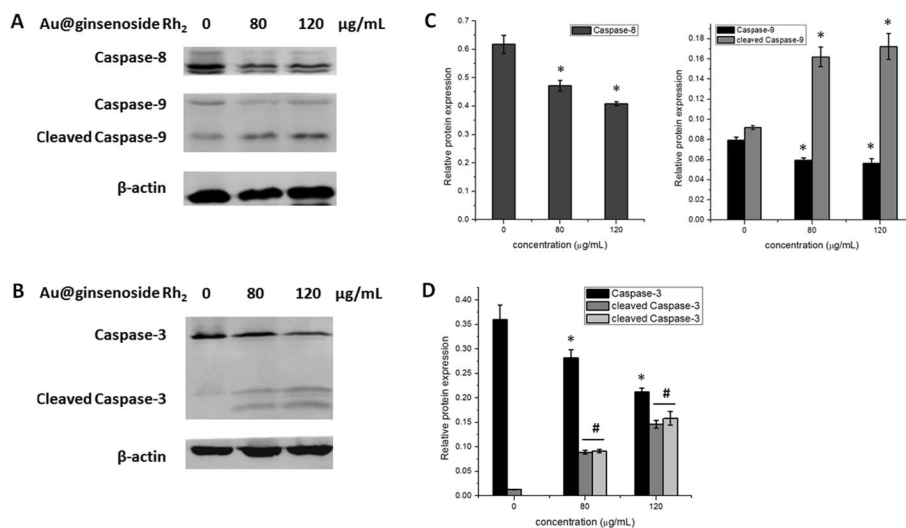
Fig. 7 Western blot analysis on Au@ginsenoside Rh_2 NPs caused expression of caspase group (caspase-3, 8, 9) which related to apoptosis of cancer cells (**A**, **B**) and the relative gray intensity (vs internal reference) of caspase-3, 8, 9 with different concentrations of Au@ginsenoside Rh_2 NPs in A375 cells (**C**, **D**). Results indicated the apoptosis of A375 cells has been certainly induced after treating with Au@ginsenoside Rh_2 NPs (*$p < 0.05$ vs control group, #$p < 0.05$ vs control group, consider the two bands of cleaved caspase-3 as one group)

working mechanisms of ginsenoside Rh_2-reduced AuNPs with enhanced anticancer activity. Therefore, owning to the remarkable anticancer property of herbal drug functionalized Au@ginsenoside Rh_2 NPs, it is reasonable to believe that the as-prepared nanoparticles will have effective utility and valuable applications in biomedical fields. It will also promote the development of multifunctional TCM-modified nanocomposites in the field of cancer therapy.

Materials and methods

Chemical and reagent

Ginsenoside Rh_2 (> 98%) was isolated from *Panax ginseng* C.A. Meyer by our group and identified by nuclear magnetic resonance (NMR), HPLC and MS based on data reported in the literature (Huang et al. 2008). Hypochlorous acid ($HAuCl_4$, > 99.8%) were purchased from Sinopharm Chemicals Reagent Co., Ltd (Shanghai, China). Analytical grade reagents, such as sodium citrate (SC, > 99.5%) and hydrochloric acid (HCl, 37%), anhydrous ethanol etc. were obtained from Beijing Chemical Works (Beijing, China). Distilled and deionized water of 18.2 MΩ cm were used in experiments. Dimethyl sulfoxide (DMSO, > 99.9%), tris (hydroxymethyl) aminomethane (Tris, > 99.9%), glycine (> 99.9%) and phenylmethanesulfonyl fluoride (PMSF, > 99.9%) were molecular biology grade and bought from Sangon Biotech. Co., Ltd (Shanghai, China). Radio Immunoprecipitation Assay (RIPA) lysis buffer, Sodium dodecyl sulfate (SDS, > 99.9%) was from Beyotime Biotechnology Co. (Shanghai, China). Skim milk powder was purchased from Becton, Dickinson and Company (BD Corporation, NJ, USA). Primary antibodies such as β-actin, caspase-3, 8, 9 and fluorescence labeling secondary antibodies were from Cell Signaling Technology Inc (MA, USA). For cell culture, Gibco Dulbecco's modified Eagle medium (DMEM) with high glucose and fetal bovine serum (FBS) from Thermo Fisher Scientific Corporation (Waltham, MA, USA) were applied to experiments with the concentration of 100 U/mL penicillin and 100 μg/mL streptomycin. Trypsin with 0.02% EDTA was purchased from Biosharp Company (Beijing, China). Phosphate buffer saline (PBS, 1×, pH 7.4) will be equilibrated at 37 ℃ before use.

Synthesis of Au@ginsenoside Rh_2 NPs

According to the previously reported seed-mediated method, highly monodisperse citrate-stabilized Au nanoparticles were prepared beforehand as seeds for subsequent Au nanoparticles growth (Herizchi et al. 2016). The 7.5 μmol $HAuCl_4$ was dissovled in 30 mL deionized water and heated in an erlenmeyer flask to 100 ℃. Then 900 μL sodium citrate (2% w/v) was added to this solution. After 30 min reaction, when it turned to wine red, Au nanoparticles with the diameter about 30–40 nm were prepared for subsequent reactions used as seeds. The preparation of Au@ginsenoside Rh_2 NPs was performed at room temperature using Au seed-mediated method. In a typical preparation, 10 μmol $HAuCl_4$ was added into the 10 mL double-distilled water containing 300 μL as-prepared Au seeds as the growth solution, then 3 μmol ginsenoside Rh_2 solution was added into the growth solution (molar ratio of $HAuCl_4$ to ginsenoside Rh_2 was 10:3). After the growth solution stirring in room temperature for 2 h, the growth solution gradually turned to violet while the Au@ginsenoside Rh_2 NPs was formed. Finally the

solution was purified by centrifuging at 5000 rpm for 10 min and washed with double deionized water.

Characteristics of Au@ginsenoside Rh$_2$ NPs

UV–visible absorption of nanoparticles was observed by Shimadzu 2600 UV–vis–NIR spectrophotometer (Shimadzu Co., Tokyo, Japan) at room temperature. Transmission electron microscopy (TEM) was performed using the Hitachi H-800 electron microscope (Hitachi, Ltd., Tokyo, Japan) at 200 kV acceleration voltages with a CCD camera. Fourier-transform infrared (FT-IR) spectroscopy was performed with a Nicolet AVATAR 360 type FT-IR spectrometer from Thermo Fisher Scientific. Dynamic light scattering (DLS) measurements would be operated by Zetasizer NanoZS (Malvern Instruments Ltd., Worcestershire, UK). Agilent 1200 series HPLC system (Agilent Technologies, CA, USA) equipped with UV detector was operated with a Agilent ZORBAX Eclipse XDB-C$_{18}$ column (4.6 × 250 mm, 5 μm). Detection wavelength and column temperature were set at 203 nm and 30 ℃ respectively. The HPLC of mobile phase was consisted of acetonitrile (A) and water (B). And conditions should be set as follows with the flow rate of 1.0 mL/min: 0–20 min, 40(A):60(B); 20–40 min, 40(A):60(B)–60(A):40(B); 40–60 min, 60(A):40(B).

Cell culture and cellular uptake of Au@ginsenoside Rh$_2$

Human melanoma cancer cells A375 which obtained from American Type Culture Collection (ATCC, Manassas, VA, USA), were seeded on a confocal observation dish at a density of 3×10^5 cells per well and cultured with DMEM medium containing 10% FBS and 1% penicillin and streptomycin solution (100×). The incubation was carried out in a fully humidified atmosphere at 37 ℃ with 5% CO$_2$. For cell uptake analysis, the as-prepared Au@ginsenoside Rh$_2$ were labeled with FITC, which could be observed with fluorescence microscope. When cells were cultured for 24 h, complete medium with 50 μg/mL Au@ginsenoside Rh$_2$ NPs could be added into the culture system. After 6 h incubation at 37 ℃ with 5% CO$_2$, cancer cells were washed with PBS for three times and then fixed with 4% paraformaldehyde solution in dark for 30 min. Finally images were collected by Leica DMI 3000B inverted fluorescence microscope (Leica Microsystems GmbH, Wetzlar, Germany).

Cytotoxicity of Au@ginsenoside Rh$_2$ NPs on cells

Cell Counting Kit-8 (CCK-8; Dojindo Laboratories, Kumamoto, Japan) was applied in the experiment to reflect the cell viability of different cells after treating with Au@ginsenoside Rh$_2$ NPs. The assay reflected the influence of as-prepared nanomaterials on cell proliferation. In brief, human renal epithelial cells 293T and umbilical vein endothelial cells HUVEC, other cancer cell lines including HepG-2, U251, A549 and A375 were seeded in 96-well plates at a cell concentration of 8000 cells/well. After incubating for 24 h, different concentrations of Au@ginsenoside Rh$_2$ NPs were added in the plates. After another 24 h treatment, the medium of each well was replaced with a fresh one which contained 10% of CCK-8 solution. Then 96-well plates were continuously incubated at 37 ℃, 5% CO$_2$ for 1 h. Optical Density (OD) at 450 nm was obtained by the microplate reader.

Lactate dehydrogenase (LDH) release assay

Cell damage can be reflected by assay of released LDH. As a stable cytoplasmic enzyme present in all types of cells, LDH will release into the culture medium through damaged plasma membrane. The amount of the formazan dye thus formed is proportional to the amount of LDH released into the cell supernatant, which indicates cell membrane integrity or cytotoxicity. The LDH Release Assay Kit (Beyotime Biotechnology, Shanghai, China) was used in this experiment. Briefly, cells in 96-well plates were incubated with different concentrations of Au@ginsenoside Rh_2 NPs in low FBS culture medium for 24 h. Then 20 μL of the lysis buffer was added to each well of the high control group at 1 h before the scheduled test time. The plate was continued to incubate at 37 °C in a 5% CO_2 incubator. After centrifuging the plate at $400 \times g$ for 5 min to precipitate the cells, 100 μL of the supernatant was transferred from each well to a new clear 96-well plate. And 100 μL of the working solution was added to each well. After incubating in dark at room temperature for 30 min, 50 μL of the stop solution was added to each well. Then, the absorbance was measured at 490 nm by a microplate reader.

Cell apoptosis assay of cancer cells treated with Au@ginsenoside Rh_2 NPs

Apoptosis Assay was detected by flow cytometry (FCM). A375 cells were seeded in 6-well plates at an initial density of 5×10^5 cells/well and incubated for 24 h. Then cells were incubated with different concentration of Au@ginsenoside Rh_2 for 24 h. After the treatment, the Annexin V-FITC/PI Apoptosis Analysis Kit (Sungene Biotech Co., Tianjin, China) was applied to the experiment. Binding buffer ($10\times$) should be diluted to working concentration ($1\times$) with distilled water. Cancer cells were harvested and washed twice with precooled PBS (pH 7.4). Then cells were suspended in 1 mL $1\times$ Binding Buffer and centrifuged at $300 \times g$ for 10 min. Binding Buffer should be removed from the cell pellet and resuspend in 100 μL of binding buffer. After adding 5 μL of Annexin V-FITC to the system, each sample should be gently vortexed and incubated for 10 min at room temperature. Then 5 μL solution of PI was also added in the system and incubated for 5 min. Finally, PBS was added to get a 500 μL reaction system and vortexed gently. Samples should be analyzed by Cytomics™ FC 500 flow cytometer (Beckman Coulter Co., Brea, CA, USA) within 1 h. Operating procedures should be avoided from light.

ROS quantification of cancer cells treated with Au@ginsenoside Rh_2 NPs

The Intracellular ROS levels were detected by a flow cytometer (Beckman Coulter Inc., Fullerton, CA, USA), using 2′,7′-Dichlorodihydrofluorescein diacetate (DCFH-DA) as the fluorescent probe. DCFH-DA can be cleaved by nonspecific esterases to generate DCFH. Then DCFH will oxidize into the fluorescent compound DCF by ROS quantitatively. So in the present assay, protocol was shown below. Cancer cells with the concentration of 2.5×10^5 cells/mL should be seeded in 6-well plates. After incubating with different concentrations of Au@ginsenoside Rh_2 NPs for 24 h, cells of each sample were collected and Reactive Oxygen Species Assay Kit (Beyotime Biotechnology, Shanghai, China) was used for detecting the ROS level. Detection probes were diluted in proportion of 1:1000 and separately added to each sample. After 30 min incubation at 37 °C

in dark, samples should be washed with serum-free medium three times for removing excessive detection probes. Then the generation of ROS in living cells could be measured by flow cytometry.

High content imaging analysis

High-content imaging, which based on cell culture plates scanning and automated fluorescence microscopy techniques, has become a visualized routine in cellular states identification and researches of toxicology and drug discovery. In this investigation, to further reflect the anticancer effect of Au@ginsenoside Rh$_2$ NPs, we used the Operetta CLS™ High-Content Imaging System (PerkinElmer Inc., MA, USA) to obtain the images. The staining was carried out by an apoptosis and necrosis assay kit (Beyotime Biotechnology, Shanghai, China). Cells were seeded in 96-well plates and cultured with different concentrations of Au@ginsenoside Rh$_2$ NPs for 24 h. Then we removed the supernatant and washed the adherent cells with cold PBS. Cancer cells were labeled with Hoechst 33342 and propidium iodide (PI) for 30 min at 4 °C under working concentration. Redundant dye liquor was removed by washing with PBS thrice. As we tried to investigate the effect of ROS on apoptosis, the groups which treated with Au@ginsenoside Rh$_2$ NPs containing antioxidant *N*-acetyl-L-cysteine (NAC, 5 mmol/L) were taken as comparison.

Cell cycle analysis of Au@ginsenoside Rh$_2$ NPs treated cancer cells

The cell culture process and the treatment with Au@ginsenoside Rh$_2$ were the same as apoptosis assay. After the treatment with different concentration of the NPs, A375 cells were harvested and washed with pre-cooled PBS for twice. Then the cells were preserved in 70% ice-chilled alcohol at -20 °C for long-term fixing. When we started the cell cycle detection, the fixed cells were centrifuged for collection and washed twice with PBS. Then A375 cells were resuspended in 0.5 mL of staining solution containing 50 μg/mL PI solution, 100 μg/mL RNase A, and 0.2% Triton X-100, and then the samples was protecting from light for 30 min. The cells were then analyzed by a Beckman Coulter FC 500 flow cytometer.

Wound scratch test for cell migration analysis

We conducted the wound scratch test for investigating the effect of Au@ginsenoside Rh$_2$ NPs on the cancer cell migration. In brief, cancer cells were seeded in 12-well plates and cultivated with the complete medium. After the well plates were covered with 80–90% confluent monolayer cells, we scratched the cancer cells surface to form uniform wounds by 10 μL pipette tips. Then each well plate was flushed with PBS thrice to remove the cellular debris and floating cells. DMEM containing 2% FBS (v/v) with different concentrations of Au@ginsenoside Rh$_2$ NPs was used for cell culture in the following steps. The initial wound and migration of cancer cells in scratched area should be observed with an interval of 12 h (at the time of 0 h and 24 h) and photographed under the Olympus inverted microscope for 24 h (Tokyo, Japan). At least three different fields from each sample were acquired and should be quantitatively estimated and analyzed by the changes of the wound width.

Cell invasion assay

To assess the invasion ability of cancer cells, the Transwell chambers with 8.0 μm porous polycarbonate membranes (Corning-Costar, NY, USA) were used following by instructions of the manufacturer. This assay could examine the capacity of cells for invading through the Matrigel-coated filter. Firstly, A375 cancer cells were pretreated with different concentration of Au@ginsenoside Rh_2 NPs for 24 h. Then a total 2×10^4 of the pretreated cells were added to each upper chamber and cultured with serum-free DMEM medium. The lower chambers should be added with 500μL DMEM medium containing 10% FBS. After incubation for 24 h, cancer cells remaining on the upper surface of the filter were removed by cotton tips. Cells that invaded to another side of the membrane were fixed with 4% paraformaldehyde for 30 min and then stained with 0.1% crystal violet solution for 30 min. We counted the number of cells in random fields under a microscope (Olympus Co, Tokyo, Japan). Results would be expressed by images and average number of cells/field of view compared with the control group.

Western blot analysis of Au@ginsenoside Rh_2 NPs treated cancer cells

We took western bolt assay to reflect the expression of apoptosis-related protein. Cancer cells treated with different concentrations of Au@ginsenoside Rh_2 NPs. RIPA lysis and extraction buffer containing 10% PMSF was used for getting protein samples. After detecting for the protein concentration with BCA protein assay kit, we mixed the extract with loading buffer for further electrophoresis. In brief, 50 μg protein samples were loaded on 12% SDS-polyacrylamide gelelectrophoresis (SDS-PAGE) gels and transferred to a polyvinylidene difluoride (PVDF) membrane (Merck Millipore Co., MA, USA). After using 5% skim milk as blocking solution, membranes were divided according to the protein markers and incubated with different primary antibodies over night under 4 °C respectively. Specific fluorescent-labeled secondary antibodies were reacted on membranes in dark for about 1 h. Results were detected by Odyssey infrared imaging system (LI-COR Biosciences, NE, USA) after washing off the uncombined antibodies for three times. According to the manufacture's protocol, primary antibody dilution ratio was 1:1000 for β-actin and caspase 3, 8, 9. And the dilution factors of secondary antibody were 1:10,000.

Statistical analysis

All the analysis data were carry out in triplicate observations. Final values were presented as mean ± SD. Statistical significance was determined by one-way ANOVA followed by Tukey comparison tests, using the SPSS 26.0 software (SPSS Inc., Chicago, IL, USA). Results were considered statistically significant if the $p < 0.05$.

Supplementary Information

The online version contains supplementary material available at https://doi.org/10.1186/s12645-022-00142-x.

Additional file 1: Characterization of Au@ginsenoside Rh_2 NPs and results of cell uptake and cell proliferation.

Declarations

Competing interests

The authors report no conflicts of interest in this work.

References

Al Saqr A, Khafagy ES, Alalaiwe A, Aldawsari MF, Alshahrani SM, Anwer MK, Khan S, Lila ASA, Arab HH, Hegazy WAH (2021) Synthesis of gold nanoparticles by using green machinery: characterization and in vitro toxicity. Nanomaterials 11:808

Alphandery E (2020) Natural metallic nanoparticles for application in nano-oncology. Int J Mol Sci 21:4412

Boomi P, Ganesan RM, Poorani G, Gurumallesh Prabu H, Ravikumar S, Jeyakanthan J (2019) Biological synergy of greener gold nanoparticles by using *Coleus aromaticus* leaf extract. Mater Sci Eng C Mater Biol Appl 99:202–210

Brown T, Sykes D, Allen AR (2021) Implications of breast cancer chemotherapy-induced inflammation on the gut, liver, and central nervous system. Biomedicines 9:189

Cheung KL, Chen H, Chen Q, Wang J, Ho HP, Wong CK, Kong SK (2012) CTAB-coated gold nanorods elicit allergic response through degranulation and cell death in human basophils. Nanoscale 4:4447–4449

Choi WY, Lim HW, Lim CJ (2013) Anti-inflammatory, antioxidative and matrix metalloproteinase inhibitory properties of 20(R)-ginsenoside Rh2 in cultured macrophages and keratinocytes. J Pharm Pharmacol 65:310–316

da Silva AB, Rufato KB, de Oliveira AC, Souza PR, da Silva EP, Muniz EC, Vilsinski BH, Martins AF (2020) Composite materials based on chitosan/gold nanoparticles: from synthesis to biomedical applications. Int J Biol Macromol 161:977–998

Ding X, Li D, Jiang J (2020a) Gold-based inorganic nanohybrids for nanomedicine applications. Theranostics 10:8061–8079

Ding Y, Xu H, Xu C, Tong Z, Zhang S, Bai Y, Chen Y, Xu Q, Zhou L, Ding H et al (2020b) A nanomedicine fabricated from gold nanoparticles-decorated metal-organic framework for cascade chemo/chemodynamic cancer therapy. Adv Sci 7:2001060

El-Sahli S, Hua K, Sulaiman A, Chambers J, Li L, Farah E, McGarry S, Liu D, Zheng P, Lee SH et al (2021) A triple-drug nano-therapy to target breast cancer cells, cancer stem cells, and tumor vasculature. Cell Death Dis 12:8

Fratoddi I (2017) Hydrophobic and hydrophilic Au and Ag nanoparticles. Breakthroughs and perspectives. Nanomaterials 8:11

Fu BD, Bi WY, He CL, Zhu W, Shen HQ, Yi PF, Wang L, Wang DC, Wei XB (2013) Sulfated derivatives of 20(S)-ginsenoside Rh2 and their inhibitory effects on LPS-induced inflammatory cytokines and mediators. Fitoterapia 84:303–307

Ginzburg AL, Truong L, Tanguay RL, Hutchison JE (2018) Synergistic toxicity produced by mixtures of biocompatible gold nanoparticles and widely used surfactants. ACS Nano 12:5312–5322

Giraldez-Perez RM, Grueso E, Dominguez I, Pastor N, Kuliszewska E, Prado-Gotor R, Requena-Domenech F (2021) Biocompatible DNA/5-fluorouracil-gemini surfactant-functionalized gold nanoparticles as promising vectors in lung cancer therapy. Pharmaceutics 13:423

Herizchi R, Abbasi E, Milani M, Akbarzadeh A (2016) Current methods for synthesis of gold nanoparticles. Artif Cells Nanomed Biotechnol 44:596–602

Hou J, Xue J, Wang Z, Li W (2018) Ginsenoside Rg3 and Rh2 protect trimethyltin-induced neurotoxicity via prevention on neuronal apoptosis and neuroinflammation. Phytother Res 32:2531–2540

Hsieh YH, Deng JS, Chang YS, Huang GJ (2018) Ginsenoside Rh2 ameliorates lipopolysaccharide-induced acute lung injury by regulating the TLR4/PI3K/Akt/mTOR, Raf-1/MEK/ERK, and Keap1/Nrf2/HO-1 signaling pathways in mice. Nutrients 10:1208

Huang J, Tang XH, Ikejima T, Sun XJ, Wang XB, Xi RG, Wu LJ (2008) A new triterpenoid from *Panax ginseng* exhibits cytotoxicity through p53 and the caspase signaling pathway in the HepG2 cell line. Arch Pharm Res 31:323–329

Hurh J, Markus J, Kim Y-J, Ahn S, Castro-Aceituno V, Mathiyalagan R, Kim YJ, Yang DC (2017) Facile reduction and stabilization of ginsenoside-functionalized gold nanoparticles: optimization, characterization, and in vitro cytotoxicity studies. J Nanoparticle Res 19:1–13

Hwang JT, Kim SH, Lee MS, Kim SH, Yang HJ, Kim MJ, Kim HS, Ha J, Kim MS, Kwon DY (2007) Anti-obesity effects of ginsenoside Rh2 are associated with the activation of AMPK signaling pathway in 3T3-L1 adipocyte. Biochem Biophys Res Commun 364:1002–1008

Khan T, Ullah N, Khan MA, Mashwani ZU, Nadhman A (2019) Plant-based gold nanoparticles; a comprehensive review of the decade-long research on synthesis, mechanistic aspects and diverse applications. Adv Coll Interface Sci 272:102017

Yao *et al. Cancer Nanotechnology*   (2022) 13:35

Page 18 of 18

Khursheed R, Dua K, Vishwas S, Gulati M, Jha NK, Aldhafeeri GM, Alanazi FG, Goh BH, Gupta G, Paudel KR et al (2022) Biomedical applications of metallic nanoparticles in cancer: current status and future perspectives. Biomed Pharmacother = Biomedecine & Pharmacotherapie 150:112951

Kuchur OA, Tsymbal SA, Shestovskaya MV, Serov NS, Dukhinova MS, Shtil AA (2020) Metal-derived nanoparticles in tumor theranostics: potential and limitations. J Inorg Biochem 209:111117

Kumar A, Das N, Satija NK, Mandrah K, Roy SK, Rayavarapu RG (2019) A novel approach towards synthesis and characterization of non-cytotoxic gold nanoparticles using taurine as capping agent. Nanomaterials 10:45

Li C, Gao H, Feng X, Bi C, Zhang J, Yin J (2020a) Ginsenoside Rh2 impedes proliferation and migration and induces apoptosis by regulating NF-kappaB, MAPK, and PI3K/Akt/mTOR signaling pathways in osteosarcoma cells. J Biochem Mol Toxicol 34:e22597

Li C, Mei E, Chen C, Li Y, Nugasur B, Hou L, Ding X, Hu M, Zhang Y, Su Z et al (2020b) Gold-nanobipyramid-based nanotheranostics for dual-modality imaging-guided phototherapy. ACS Appl Mater Interfaces 12:12541–12548

Li X, Chu S, Lin M, Gao Y, Liu Y, Yang S, Zhou X, Zhang Y, Hu Y, Wang H, Chen N (2020c) Anticancer property of ginsenoside Rh2 from ginseng. Eur J Med Chem 203:112627

Liu H, Yang Y, Liu Y, Pan J, Wang J, Man F, Zhang W, Liu G (2020a) Melanin-like nanomaterials for advanced biomedical applications: a versatile platform with extraordinary promise. Adv Sci 7:1903129

Liu X, Zhang M, Yan D, Deng G, Wang Q, Li C, Zhao L, Lu J (2020b) A smart theranostic agent based on Fe-HPPy@Au/DOX for CT imaging and PTT/chemotherapy/CDT combined anticancer therapy. Biomater Sci 8:4067–4072

Lu C, Wang Y, Lv J, Jiang N, Fan B, Qu L, Li Y, Chen S, Wang F, Liu X (2018) Ginsenoside Rh2 reverses sleep deprivation-induced cognitive deficit in mice. Behav Brain Res 349:109–115

Matur M, Madhyastha H, Shruthi TS, Madhyastha R, Srinivas SP, Navya PN, Daima HK (2020) Engineering bioactive surfaces on nanoparticles and their biological interactions. Sci Rep 10:19713

Nag SA (2012) Ginsenosides as anticancer agents: in vitro and in vivo activities, structure–activity relationships, and molecular mechanisms of action. Front Pharmacol 3:25

Park EK, Choo MK, Kim EJ, Han MJ, Kim DH (2003) Antiallergic activity of ginsenoside Rh2. Biol Pharm Bull 26:1581–1584

Qiao J, Qi L (2021) Recent progress in plant-gold nanoparticles fabrication methods and bio-applications. Talanta 223:121396

Rao KM, Kumar A, Suneetha M, Han SS (2018) pH and near-infrared active; chitosan-coated halloysite nanotubes loaded with curcumin-Au hybrid nanoparticles for cancer drug delivery. Int J Biol Macromol 112:119–125

Ratan ZA, Haidere MF, Hong YH, Park SH, Lee JO, Lee J, Cho JY (2021) Pharmacological potential of ginseng and its major component ginsenosides. J Ginseng Res 45:199–210

Ronavari A, Igaz N, Adamecz DI, Szerencses B, Molnar C, Konya Z, Pfeiffer I, Kiricsi M (2021) Green silver and gold nanoparticles: biological synthesis approaches and potentials for biomedical applications. Molecules 26:844

Ru W, Wang D, Xu Y, He X, Sun YE, Qian L, Zhou X, Qin Y (2015) Chemical constituents and bioactivities of *Panax ginseng* (C. A. Mey.). Drug Discov Ther 9:23–32

Tarantola M, Pietuch A, Schneider D, Rother J, Sunnick E, Rosman C, Pierrat S, Sonnichsen C, Wegener J, Janshoff A (2011) Toxicity of gold-nanoparticles: synergistic effects of shape and surface functionalization on micromotility of epithelial cells. Nanotoxicology 5:254–268

Wang H, Yu P, Gou H, Zhang J, Zhu M, Wang ZH, Tian JW, Jiang YT, Fu FH (2012a) Cardioprotective effects of 20(S)-ginsenoside Rh2 against doxorubicin-induced cardiotoxicity in vitro and in vivo. Evid Based Complement Altern Med 2012:506214

Wang Y, Wang H, Liu Y, Li C, Qi P, Bao J (2012b) Antihyperglycemic effect of ginsenoside Rh2 by inducing islet beta-cell regeneration in mice. Horm Metab Res = Hormon- Und Stoffwechselforschung = Hormones Et Metabolisme 44:33–40

Wang W, Tang Q, Yu T, Li X, Gao Y, Li J, Liu Y, Rong L, Wang Z, Sun H et al (2017) Surfactant-free preparation of Au@Resveratrol hollow nanoparticles with photothermal performance and antioxidant activity. ACS Appl Mater Interfaces 9:3376–3387

Wang L, Xu J, Yan Y, Liu H, Li F (2019a) Synthesis of gold nanoparticles from leaf *Panax notoginseng* and its anticancer activity in pancreatic cancer PANC-1 cell lines. Artif Cells Nanomed Biotechnol 47:1216–1223

Wang Z, Kim U, Jiao Y, Li C, Guo Y, Ma X, Jiang M, Jiang Z, Hou Y, Bai G (2019b) Quantitative proteomics combined with affinity MS revealed the molecular mechanism of ginsenoside antitumor effects. J Proteome Res 18:2100–2108

Wang Y, Li S, Wang X, Chen Q, He Z, Luo C, Sun J (2021) Smart transformable nanomedicines for cancer therapy. Biomaterials 271:120737

Wu S, Yang X, Luo F, Wu T, Xu P, Zou M, Yan J (2018) Biosynthesis of flower-shaped Au nanoclusters with EGCG and their application for drug delivery. J Nanobiotechnol 16:90

Yang L, Kim TH, Cho HY, Luo J, Lee JM, Chueng SD, Hou Y, Yin PT, Han J, Kim JH et al (2021) Hybrid graphene-gold nanoparticle-based nucleic acid conjugates for cancer-specific multimodal imaging and combined therapeutics. Adv Funct Mater 31:2006918

Zhang H, Park S, Huang H, Kim E, Yi J, Choi SK, Ryoo Z, Kim M (2021) Anticancer effects and potential mechanisms of ginsenoside Rh2 in various cancer types (Review). Oncol Rep 45:1–10

Zheng PP, Li J, Kros JM (2018) Breakthroughs in modern cancer therapy and elusive cardiotoxicity: critical research-practice gaps, challenges, and insights. Med Res Rev 38:325–376

Zhu S, Liu X, Xue M, Li Y, Cai D, Wang S, Zhang L (2021) 20(S)-ginsenoside Rh2 induces caspase-dependent promyelocytic leukemia-retinoic acid receptor A degradation in NB4 cells via Akt/Bax/caspase9 and TNF-alpha/caspase8 signaling cascades. J Ginseng Res 45:295–304

Publisher's Note